Department of Applied Physics

Electron transport in graphene nanostructures

Karri Saloriutta

Aalto University

DOCTORAL DISSERTATIONS

Aalto University publication series
DOCTORAL DISSERTATIONS 7/2013

Electron transport in graphene nanostructures

Karri Saloriutta

A doctoral dissertation completed for the degree of Doctor of Science in Technology to be defended, with the permission of the Aalto University School of Science, at a public examination held at the lecture hall E of the main building on 23 January 2013 at 13:00.

Aalto University
School of Science
Department of Applied Physics
Electronic Properties of Materials

Supervising professor
Prof. Martti J Puska

Preliminary examiners
Prof. Jouko Nieminen, TUT, Finland
Dr. Andrés Ayuela, EHU, Spain

Opponent
Prof. Kristian Thygesen, DTU, Denmark

Aalto University publication series
DOCTORAL DISSERTATIONS 7/2013

ISBN 978-952-60-4965-6 (printed)
ISBN 978-952-60-4966-3 (pdf)
ISSN-L 1799-4934
ISSN 1799-4934 (printed)
ISSN 1799-4942 (pdf)
http://urn.fi/URN:ISBN:978-952-60-4966-3

Unigrafia Oy
Helsinki 2013

Finland

441 697
Printed matter

Aalto University

Abstract

Aalto University, P.O. Box 11000, FI-00076 Aalto www.aalto.fi

Author
Karri Saloriutta

Name of the doctoral dissertation
Electron transport in graphene nanostructures

Publisher School of Science

Unit Department of Applied Physics

Series Aalto University publication series DOCTORAL DISSERTATIONS 7/2013

Field of research Computational physics

Manuscript submitted 6 November 2012 **Date of the defence** 23 January 2013

Permission to publish granted (date) 12 December 2012 **Language** English

☐ **Monograph** ☒ **Article dissertation (summary + original articles)**

Abstract

Since its first synthesis and characterization in 2004 graphene has been the focus of an intense research effort. Charge carriers in graphene are massless Dirac fermions that behave fundamentally differently than electrons in conventional semiconductor heterostructures. For applications the most interesting factor is the very high quality of the graphene lattice leading to ballistic transport over micron length scales. The transport of electrons in graphene has thus been widely studied for applications in electronics. Although bulk graphene is gapless, a gap can be generated by breaking the graphene into finite strips, graphene nanoribbons.

Our work concerns the study of electron transport in graphene and graphene nanoribbons using first principles density functional theory (DFT) and semiempirical tight-binding (TB) methods. The TB and DFT approaches are complementary in that DFT makes it possible to study small graphene structures with an accurate accounting for effects such as ionic relaxation, charge transfer and magnetism while TB can be used for fast calculations of large, disordered samples. By combining DFT and TB very accurate TB parameterizations can be generated. The parameterizations can also be generalized for magnetic systems by using the Hubbard model.

We have used these methods to study the effect various structural defects such as vacancies, adatoms and disordered edges have on the transmission properties of graphene nanostructures. We have shown that even single defect calculations are enough for estimating the conducting properties of large samples with the aid of a scaling approach to transport. This makes it possible to characterize different defects in graphene based on a scattering cross section that can be calculated directly by DFT for small systems.

Keywords graphene, electron transport, density functional theory

ISBN (printed) 978-952-60-4965-6 **ISBN (pdf)** 978-952-60-4966-3

ISSN-L 1799-4934 **ISSN (printed)** 1799-4934 **ISSN (pdf)** 1799-4942

Location of publisher Espoo **Location of printing** Helsinki **Year** 2013

Pages 92 **urn** http://urn.fi/URN:ISBN:978-952-60-4966-3

Aalto-yliopisto

Tiivistelmä

Aalto-yliopisto, PL 11000, 00076 Aalto www.aalto.fi

Tekijä
Karri Saloriutta

Väitöskirjan nimi
Elektronien kuljetusteoria grafeeninanorakenteissa

Julkaisija Perustieteiden korkeakoulu

Yksikkö Teknillisen fysiikan laitos

Sarja Aalto University publication series DOCTORAL DISSERTATIONS 7/2013

Tutkimusala Laskennallinen fysiikka

Käsikirjoituksen pvm 06.11.2012 **Väitöspäivä** 23.01.2013

Julkaisuluvan myöntämispäivä 12.12.2012 **Kieli** Englanti

☐ **Monografia** ☒ **Yhdistelmäväitöskirja (yhteenveto-osa + erillisartikkelit)**

Tiivistelmä

Grafeenia on tutkittu intensiivisesti sen jälkeen, kun sitä valmistettiin ja karakterisoitiin ensi kertaa 2004. Normaaleista puolijohteista poiketen grafeenin varauksenkuljettajat ovat massattomia Dirac-fermioneja, jotka käyttäytyvät huomattavan eri tavalla normaalien puolijohderakenteiden elektroneihin verrattuna. Grafeeni on myös herättänyt toiveita elektroniikan sovellutuksista, sillä grafeenihilan hyvästä laadusta johtuen elektronit etenevät parhaimmillaan siroamatta mikrometrin matkoja. Vaikka grafeenin vyörakenne on normaalisti aukoton, grafeenin leikkaaminen nanonauhoiksi synnyttää aukon.

Tämä väitöskirja käsittelee elektronien kuljetusteoriaa grafeenissa ja grafeeninanonauhoissa tiheysfunktionaaliteoriaan (DFT) ja semiempiiriseen tight-binding-malliin (TB) perustuen. DFT ja TB tukevat toisiaan siinä mielessä, että DFT mahdollistaa pienten rakenteiden tarkat laskut mukaanlukien ionisen relaksaation, varauksensiirron ja magneettiset ilmiöt, ja TB:llä puolestaan voidaan tutkia isoja epäjärjestäytyneitä rakenteita. Yhdistämällä DFT ja TB voidaan TB parametrisoida siten, että saavutetaan hyvin tarkkoja DFT:tä vastaavia tuloksia. TB voidaan myös yleistää magneettisille järjestelmille käyttämällä Hubbard-mallia.

Olemme käyttäneet näitä menetelmiä tutkiaksemme erilaisten rakenteellisten defektien kuten vakanssien, adatomien ja reunaepäjärjestyksen vaikutusta elektronien transmissioon. Olemme osoittaneet, että jopa yhdelle defektille tehdyistä laskuista voidaan arvioida suurten systeemien johtavuusominaiuuksia käyttämällä skaalautumiseen perustuvaa lähestymistapaa. Tämä mahdollistaa eri defektien karakterisoinnin niiden sirontavaikutusalojen perusteella. Sirontavaikutusalan puolestaan voi laskea DFT:llä suoraan yhdelle defektille.

Avainsanat grafeeni, elektronien kuljetusteoria, tiheysfunktionaaliteoria

ISBN (painettu) 978-952-60-4965-6 **ISBN (pdf)** 978-952-60-4966-3

ISSN-L 1799-4934 **ISSN (painettu)** 1799-4934 **ISSN (pdf)** 1799-4942

Julkaisupaikka Espoo **Painopaikka** Helsinki **Vuosi** 2013

Sivumäärä 92 **urn** http://urn.fi/URN:ISBN:978-952-60-4966-3

List of Publications

This thesis consists of an overview and of the following publications which are referred to in the text by their Roman numerals.

I Yvette Hancock, Karri Saloriutta, Andreas Uppstu, Ari Harju, Martti J. Puska. Spin-Dependence in Asymmetric, V-Shaped-Notched Graphene Nanoribbons. *Journal of Low Temperature Physics*, 153, 393, October 2008.

II Yvette Hancock, Andreas Uppstu, Karri Saloriutta, Ari Harju, Martti J. Puska. Generalized tight-binding transport model for graphene nanoribbon-based systems. *Physical Review B*, 81, 245402, June 2010.

III Karri Saloriutta, Yvette Hancock, Asta Kärkkäinen, Leo Kärkkäinen, Martti J. Puska, Antti-Pekka Jauho. Electron transport in edge-disorded graphene nanoribbons. *Physical Review B*, 83, 205125, May 2011.

IV Andreas Uppstu, Karri Saloriutta, Ari Harju, Martti J. Puska, Antti-Pekka Jauho. Electronic transport in graphene-based structures: An effective cross-section approach. *Physical Review B*, 85, 041401, January 2012.

V Karri Saloriutta, Andreas Uppstu, Ari Harju, Martti J. Puska. Ab initio transport fingerprints for resonant scattering in graphene. *Physical Review B*, 86, 235417, December 2012.

Author's Contribution

Publication I: "Spin-Dependence in Asymmetric, V-Shaped-Notched Graphene Nanoribbons"

The author performed the ab initio calculations and contributed to writing the paper.

Publication II: "Generalized tight-binding transport model for graphene nanoribbon-based systems"

The author performed the ab initio calculations and contributed to writing the paper.

Publication III: "Electron transport in edge-disorded graphene nanoribbons"

The author performed all the calculations and wrote the paper with contributions from coauthors.

Publication IV: "Electronic transport in graphene-based structures: An effective cross-section approach"

The author performed the ab initio calculations and contributed to writing the paper

Publication V: "Ab initio transport fingerprints for resonant scattering in graphene"

The author performed most of the calculations and wrote the paper with contributions from coauthors.

Contents

1. Introduction

The focus of this thesis is the computational study of electron transport in graphene nanostructures. The first synthesis and characterization of monolayer graphene was described in a landmark paper by Andre Geim and Kostya Novoselov [1] in 2004. This was the starting point of the work which soon after gave them the Nobel prize in physics in 2010 [2, 3]. The merits of this paper are many. It established an easy experimental procedure, mechanical exfoliation or the Scotch tape method, for producing single and multilayered graphene. It showed that optical microscopy was enough for finding single layer graphene. It proceeded to electrically gate graphene, proving that the electric field effect could be used to continuously tune between hole doping and electron doping. Already present in this first paper was the later much discussed minimum conductivity problem: there was no insulating regime between the hole doping and electron doping. Already the first paper showed some of the peculiarities of electron transport in graphene in the form of very high mobilities, long range ballistic transport and a linear energy dispersion. Quickly after this came the proof that the charge carriers in graphene are actually well described as *massless Dirac fermions* [4, 5] leading to a great deal of theoretical interest in the novel material.

As is often the case in science, there exists a rich prehistory of experimental and theoretical graphene science already prior to 2004 [2]. There were active programs in trying to produce single graphene layers through intercalation and epitaxially from silicon carbide. Some of these methods have since been refined and might be useful for future graphene electronics. Despite these advances, so far the exfoliated graphene method remains the most important way for creating graphene samples for the purposes of basic science. The concept of graphene has also long been established in the theoretical literature, first as the basis of understanding

the electronic properties of graphite [6]. The properties of Dirac fermions have thus been studied for a long time in this context [7].

In addition to the fundamental interest raised by a new type of charge carrier, graphene has also been embraced by the materials science and electronics community as an interesting material for commercial applications. Countless speculative applications for graphene have been proposed, though so far only a few have been realized in practice. Especially notable due to the high electronic quality of graphene is the fact that the hoped-for use of graphene in electronics looks rather difficult due to a lack of a band gap. Although a band gap can be created by patterning graphene into ribbons this introduces new sources of scattering due to imperfections at the edges, thus significantly decreasing the conducting properties. Bilayer graphene can also be gated to produce a band gap, but not a very large one. For these reasons it appears that graphene might be more suited for applications in either analog high speed electronics or for nanoelectromechanical systems (NEMS).

Whatever the use graphene might be put into in the future, there is a clear need for understanding the electron transport properties of graphene samples, preferably based on first principles methods with no fitting parameters. The current work shows an approach to this mostly in the context of defective graphene nanoribbons. We use density functional theory (DFT) and semiempirical tight-binding (TB) to study the coherent transmission of electrons through various different defective graphene systems.

The purpose of this introductory part of the thesis is to present the papers forming the actual new physics contributions of the thesis in the broader context of the graphene field. Since graphene research has grown so large that any sort of comprehensive review is all but impossible only those papers most relevant for the discussed physics and broad based review articles and books are cited.

This thesis introduction then consists of the following. We started with this short motivating chapter, and follow on with a basic description of the computational tools that we have used in our work, focusing on the use of DFT and semiempirical tight binding for electron transport. After introducing these tools we are able to discuss the properties of pristine bulk graphene and graphene nanoribbons as well as defective and disordered graphene and put our method development and research findings in this context. Finally, we close the thesis with some concluding remarks.

2. Computational tools

2.1 Two-probe transport

Most of the work in this thesis covers the transmission of electrons through a *two-probe* transport structure. We will first study the modeling of such structures on a general footing.

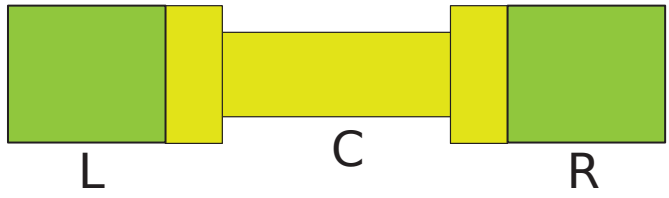

Figure 2.1. Schematic of a two-probe transport setup. A central region is sandwiched between two semi-infinite leads on both sides.

In a two-probe transport setup we consider a system like the one pictured in figure 2.1. A central region is connected to two semi-infinite leads. We describe the system with a set of local basis functions. The nature of these basis functions is not important at the moment, later we will consider both numerical atomic orbitals and a semiempirical tight binding basis but for now the most important factor is their locality. Then each basis set element belongs to just one of the regions L, C or R and the Hamiltonian becomes

$$H = \begin{pmatrix} H_{LL} & H_{LC} & 0 \\ H_{CL} & H_{CC} & H_{CR} \\ 0 & H_{RC} & H_{RR} \end{pmatrix}. \tag{2.1}$$

Here we have assumed that $H_{RL} = H_{LR} = 0$, that is, the lead regions do not couple with each other. If this is not the case we can generally always extend the central region to take in more of the lead structure so that this becomes reality. Note that while H_{CC} is a finite matrix all the other

matrices are infinite since both leads continue from the central region boundary to infinity.

We define the retarded Green's function of the system by the relation

$$(\omega I - H + i\eta^+)G^R(\omega) = I, \tag{2.2}$$

where I is the identity operator. The η^+ in this equation is an infinitesimal positive number that incorporates the boundary conditions in the equation. For a small *negative* infinitesimal η^- the equation would define the *advanced* Green's function G^A. The advanced Green's function is given by the Hermitian conjugate of the retarded Green's function, $G^A = (G^R)^\dagger$.

Writing the Green's function in the local basis we can also divide it into parts

$$G^R = \begin{pmatrix} G_{LL} & G_{LC} & G_{LR} \\ G_{CL} & G_{CC} & G_{CR} \\ G_{RL} & G_{RC} & G_{RR} \end{pmatrix}, \tag{2.3}$$

which we can then use to solve for G_{LC} and G_{RC} to get an equation for the central region

$$(\omega I_{CC} - H_{CC} - \Sigma_L - \Sigma_R)G_{CC} = I_{CC}, \tag{2.4}$$

where we have defined the left and right lead self energies

$$\Sigma_X = -H_{CX}G_{XX}H_{XC}, \tag{2.5}$$

for $X = R$ or L. Due to the local basis set the matrix H_{CX} is mostly zero and we get

$$\Sigma_X = -H_{C1}G_{11}H_{X1}, \tag{2.6}$$

where 1 denotes the *first principal layer* of the lead. The Green's function for this layer, also known as the surface Green's function, is efficiently calculated for the semi-infinite system by, for example, a recursive decimation algorithm [8] or some of the newer and faster numerical approaches based on the Krylov subspace method [9].

The effect of all these manipulations has been to embed the impact of the leads on the central region in the self-energy terms which are matrices in the central region indices only. The self-energy terms in the Hamiltonian can be thought as a pair of complex potentials that act as sources and sinks of electrons for the central region. The resulting equation (2.4) is then a finite linear matrix equation that can be readily solved to yield the central region retarded Green's function.

Although the retarded Green's function is a somewhat abstract quantity, it is nevertheless quite close to several useful and even experimentally approachable quantities. The imaginary part of the Green's function directly yields the spectral function

$$A(\omega) = i\left(G^R(\omega) - G^A(\omega)\right), \tag{2.7}$$

where $G^A = (G^R)^\dagger$ is the advances Green's function as defined above. The spectral function is a generalized density of states: the diagonal gives the local density of states while a trace gives the density of states. The local density of states is directly visible through scanning tunneling microscopy. The most important thing for our purposes, however, is the fact that we can calculate the transmission through the central region from the retarded Green's function and the self-energy matrices.

2.2 Landauer transmission formula

This work concentrates on the study of *coherent* electron transport through nanoscale graphene structures. This means that all the collisions between electrons and impurities are elastic and thus preserve the phase of the wave function. The standard approach for coherent transport in two-probe nano- and mesoscale systems is called the Landauer or the scattering approach [10].

The Landauer approach is based on the concept of transmission probability for incoming electronic states. This is typically discussed using the terminology of the scattering or S-matrix that couples the incoming and outcoming modes together. The S-matrix can be calculated based on the Green's function description of the two-probe system covered in the previous section. We give the main transmission formula here without derivation. It can be derived either based on Green's functions [11] or the Fisher-Lee relation [12]. The transmission is

$$T(\omega) = \mathrm{Tr}\{\Gamma_L G^R \Gamma_R G^A\}, \tag{2.8}$$

where $G^{R/A}$ are the retarded and advanced Green's functions of the central region. The gamma matrices are couplings to both of the leads given by the lead self-energies Σ

$$\Gamma_{L/R} = i(\Sigma^R_{L/R} - \Sigma^A_{L/R}), \tag{2.9}$$

where R and A again denote retarded and advanced self energies.

The actual conductance through the central region is then given by

$$G(\omega) = \frac{2e^2}{h} \int_{-\infty}^{\infty} (n_F(\omega - E_F^L) - n_F(\omega - E_F^R))T(\omega)d\omega \qquad (2.10)$$

where $G_0 = 2e^2/h$ is the quantum of conductance, the 2 coming from the spin degeneracy and n_F is the Fermi function.

These last sections have shown how to calculate the transmission from the infinite Hamiltonian of a two-probe system. In the semi empirical tight binding model where the Hamiltonian is explicitly known this thus gives a straightforward and easily implemented blueprint for computational transport studies. If, however, the Hamiltonian is unknown we first need a way for constructing it from first principles. One such way is provided by DFT. Conveniently the Green's function language is the same for both the tight binding formalism and the DFT, what remains is then to find out how DFT can be used to construct the Hamiltonian for a two-probe system.

2.3 Density functional theory

Before considering how a two-probe transport calculation can be performed on a first principles basis we describe briefly some of the theory and praxis of the study of the electronic structure of materials. DFT is a general way to simplify the manybody problem so that it can be solved with reasonably accuracy and limited computational time. A large amount of method and code development has turned DFT into the most widely used computational tool for electronic structure studies.

The basic idea of DFT is to forget about the complex many-body wavefunctions and deal with the electron system based on its density instead. The Hohenberg-Kohn theorem, the fundamental basis of DFT, then states that there exists a unique functional of density only whose minimum gives the ground-state of the system. The many body problem has thus been turned into a simple functional minimization task if such a functional can be found. The theoretical foundations of DFT will be omitted here and we will simply go through the main results needed for practical applications.

DFT is based on two Hohenberg-Kohn theorems which state that the electron density uniquely determines the ground state wavefunction and the exact ground state minimizes the total energy which is a functional of particle density [13]. This makes it reasonable to try to concoct a scheme to calculate the ground state density in a self-consistent manner. The

commonly used method is to solve a set of Kohn-Sham equations which represent non-interacting *quasi-particles* in an effective potential

$$\left[-\frac{\hbar}{2m}\nabla^2 + V_{\text{eff}}(\mathbf{r})\right]\phi_i(\mathbf{r}) = \epsilon_i\phi_i(\mathbf{r}), \tag{2.11}$$

where ϕ_i and ϵ_i are the Kohn-Sham orbitals and energies of the system and the effective potential is given by

$$V_{\text{eff}}(\mathbf{r}) = V_{\text{ion}}(\mathbf{r}) + \int d\mathbf{r}\frac{n(\mathbf{r})}{|\mathbf{r}-\mathbf{r}'|} + V_{\text{xc}}(\mathbf{r}). \tag{2.12}$$

Here V_{ion} is the potential due to the nuclei and the integral term is the classical Hartree self-energy of the electrons. The effective potential also contains the exchange-correlation potential V_{xc}. This potential contains the many-body effects of the electron gas and has to be approximated. The most fundamental approximation for exchange and correlation is the local density approximation (LDA) in which V_{xc} is locally approximated by the exchange-correlation potential of a homogeneous electron gas with density $n(\mathbf{r})$. This many-body potential of the homogeneous gas can be calculated by correlated many-particle techniques like quantum Monte Carlo methods and then parameterized for use in DFT calculations.

In practise DFT is used with one of several more or less standard packages. These typically have different ways of implementing the basic DFT formalism, some of these design choices having far reaching implications on the use of the code in question. The most fundamental choice is probably that of the basis set, that is how exactly are the eigenfunctions of the equation (2.11) expanded. This can be done by plane waves (for example the package VASP [14]), local orbitals (SIESTA) or real space grids (GPAW [15]), just to mention some common choices. Other choices are things like full-electron versus pseudopotential code or the exact type of the pseudopotential. Recently also the inclusion of various methods and techniques building on top of the basic DFT routines have become an important distinction between different codes. Things such as ab initio electron transport and post-DFT methods like GW or time-dependent DFT are often built on top of the regular computational framework provided by the base DFT code depending on the precise focus of the code. Codes also differ in their licencing terms, some are fully commercial or free for academic use while others are open source.

In this thesis we have mainly used the SIESTA package and especially its generalization for the two-probe transport problem, TRANSIESTA.

2.4 SIESTA and TRANSIESTA

All the DFT calculations in this thesis were done with the SIESTA DFT package [16, 17, 18]. SIESTA is a widely used DFT code that uses numeric atomic orbitals as a basis set and nonlocal pseudopotentials to deal with the core electrons. This means that the eigenfunctions are expanded as a linear combination of numerical atomic orbitals for each atom I located at $\mathbf{R}_I$

$$\Psi_{Ilmn}(\mathbf{r}) = \psi_{Iln}(r_I)Y_{lm}(\hat{\mathbf{r}}_\mathbf{I}), \tag{2.13}$$

for $\mathbf{r}_I = \mathbf{r} - \mathbf{R}_I$ and $\hat{\mathbf{r}}_\mathbf{I} = \mathbf{r}_\mathbf{I}/r_I$. This consists of a radial part ψ and a spherical harmonic Y_{lm}. The radial part of the wave function can in principle be some arbitrarily chosen local function, for example it can be optimized to yield some particular desired result. SIESTA also includes an automatic mechanism for generating basis sets by the energy shift process. Here the radial part is found by solving

$$\left(-\frac{1}{2r}\frac{d}{dr^2} + \frac{l(l+1)}{2r^2} + V_l(r)\right)\psi_l(r) = (\epsilon_l + \delta\epsilon_l)\psi_l(r), \tag{2.14}$$

where $\delta\epsilon$ is the energy shift, which can be chosen by for example minimizing the ground state energy of the system. The basis generated by including only the ψ_l from this equation is called the single-ζ or SZ basis.

Increasing of the basis set size from just the "physical" angular momentum eigenstates can be done in two different ways. First by adding polarization orbitals, that is orbitals of higher angular momentum than those in the valence. Actual physical polarization orbitals, i.e. those solved from (2.14) by increasing l by one, turn out to be too extended and sometimes even unbound and clearly cannot be used. Localized polarization orbitals can however be constructed from the radial Scrödinger equation for the highest angular momentum in an external electric field. The resulting function is then multiplied by Y_{l+1m} and added to the basis set, thus yielding the single-ζ-polarization or SZP basis.

The second way to increase the size of the basis set is by using two radial functions for each angular momentum. This is done by the split-valence method. Here the additional orbitals are smooth polynomials inside a radius r_l^s and have tail-behavior like the first-ζ orbitals. The radius is set by fixing the norm of the orbital outside the radius r_l^s. This "split norm" is then the other major parameter in addition to the energy shift for automatic basis set generation. The doubling of the basis set in this way yields the double-ζ (DZ) or the double-ζ-polarization (DZP) basis.

In the calculations done for this thesis structural relaxations are typically performed with a DZP basis while transport is calculated with the SZP basis. This is a practical compromise between accuracy and efficiency. Even higher accuracy basis sets can in principle be generated by following the procedures outlined before to get triple-ζ and double polarization orbitals but in practice it might be a good idea to use a code with a plane wave basis set such as VASP if very high accuracy is desired.

Things that cannot be represented by the LCAO basis such as the exchange-correlation potentials are described by an uniform real-space grid, the density of which is typically given by the equivalent plane-wave cutoff in Rydberg. The electrostatic Hartree potential is calculated by a fast Fourier transform. For periodic systems the first Brillouin zone can be sampled with the Monkhorst-Pack sampling [19].

To calculate electron transport with DFT we use the TRANSIESTA package, now a standard part of the SIESTA DFT code [20]. In many ways TRANSIESTA operates like an implementation of the tight-binding transport formalism presented before. The use of DFT and especially the possibility to use a bias voltage, that is, a linear voltage drop between the electrodes, just complicates things slightly.

A TRANSIESTA calculation proceeds in three parts. First the electronic structure of the leads is calculated with a standard periodic DFT calculation to get the density matrix and the Hamiltonian for the infinite leads which are saved for the subsequent steps.

Next a standard periodic SIESTA calculation is performed for a system that includes the central region and the leads. This yields the Hamiltonian and density matrix for the central region. Next the Hamiltonian for the leads and the central region is used to calculate the retarded Green's function for the system with the leads embedded using the self energies as for discussed before. The density is calculated by integrating over the retarded Green's function using an efficient contour integration technique that requires only a few energy points. This yields a Hamiltonian for the central region. A separate self consistent iteration for the Green's function makes it possible to calculate the electronic structure for a system with a finite bias voltage between the electrodes.

The third part of the calculation is the actual transmission calculation, done with an external utility TBTrans. This utility works as was discussed before for two-probe transport by first calculating the self-energies for the needed energies and then calculating the transmission based on

equation (2.8).

All the calculations included in this thesis work have been done without the bias voltage. Its inclusion is in principle simple, the potential in the leads is increased and decreased by a rigid shift and a ramp potential from left lead to right lead is added to the central region.

Other ab initio programs capable of the type of calculations discussed here include Smeagol [21], also based on SIESTA, GPAW using a SIESTA-inspired optional numerical atomic orbital basis set and Wannier90 [22] using Wannier functions generated from a variety of plane-wave basis codes. Transport calculations based on the Landauer formula have been widely utilized in the literature for various systems. One limit of the method is that it limits the studied geometry to a linear quasi-1D setup even though the systems can be periodic in the transverse direction. One alternative computational method that works well for bulk systems is the real-space Kubo-Greenwood method [23]. This method has been widely used to study transport in graphene [24, 25, 26].

2.5 Beyond DFT

The theoretical formulation presented here is unfortunately not without some fundamental problems [27, 28]. The difficulties come from the fact that the two-probe transport setup we have discussed is in fact a complicated problem of nonequilibrium statistical physics [29]. Since the central region is not in equilibrium we do not have a variational ground-state in the region either. The lack of this variational principle in turn means that the basis of DFT, the Hohenberg-Kohn theorem, is not valid. The use of DFT in the non-equilibrium setting of a quantum transport device cannot therefore be justified on theoretical grounds. The justification then has to be a practical one: often we can get at least a qualitative understanding of transport processes with NEGF-DFT in cases where other more exact methods are too cumbersome. And often enough we get results which closely match experimental data.

The whole enterprise of dividing the scattering problem to leads which are in equilibrium and a central non-equilibrium molecular region has also been criticized [30]. This dividing technique, based on the work of Caroli *et al.* on transport in metal-insulator-metal tunneling junctions [11], can be replaced by a partition-free approach by Cini [31]. A time-dependent version of the density-function theory (TDDFT) can be

combined with this approach allowing for a more rigorous *ab initio* formulation of the transport problem [30, 32]. The downside of this formulation is increased computational cost, it has to date been used only with one-dimensional test systems.

There are also other approaches than the full TDDFT treatment to improve on the plain NEGF-DFT. One is the so-called GW approximation, which has recently been used to deal with transport systems [33]. The GW approximation provides a better picture of a correlated electron system and thus makes it possible to study many interesting properties of correlated transport systems such as the Kondo effect.

3. Pristine graphene

3.1 Bulk graphene

A basic understanding of the electronic structure of graphene starts from a tight-binding model. This was studied already in 1947 by Wallace et al. [6] to understand the electronic properties of graphite. The core electrons can be safely forgotten and only the four valence electrons are considered. Three of these are bound tightly with neighboring atoms forming directional σ bonds. This leaves only the p_z orbitals, which form delocalized π bonds with each other.

Figure 3.1 shows a view of a graphene sheet and the first Brillouin zone of the reciprocal lattice. The graphene lattice is a bipartite lattice, there are two atoms, marked A and B in the schematic, forming two sublattices. The shaded area shows the primitive unit cell. The hexagonal first Brillouin zone shows six high symmetry K-points two of which are unequal since they cannot be connected with a reciprocal lattice vector, typically called K and K'.

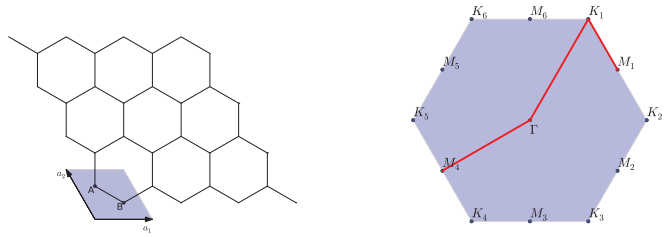

Figure 3.1. Schematic view of a graphene lattice showing the primitive cell and the first Brillouin zone of the reciprocal lattice. The Brillouin zone shows the band-path plotted in figure 3.2

.

The nearest neighbor Hamiltonian can be written

$$H = \sum_{\langle i,j \rangle} t c_i^\dagger c_j + H.c., \tag{3.1}$$

where t is the hopping element and we sum over pairs of nearest neighbors and the onsite energy has been set to zero. This Hamiltonian can then be solved to get the dispersion

$$\epsilon(\mathbf{k}) = \pm t \sqrt{1 + 4\cos\frac{ak_x}{2}\cos\frac{\sqrt{3}k_y}{2} + 4\cos^2\frac{ak_x}{2}}, \tag{3.2}$$

where a is the lattice constant of around 2.46 Å. The only points where the conductance and valence bands meet is at the K-points where $\epsilon(K) = \epsilon(K') = 0$.

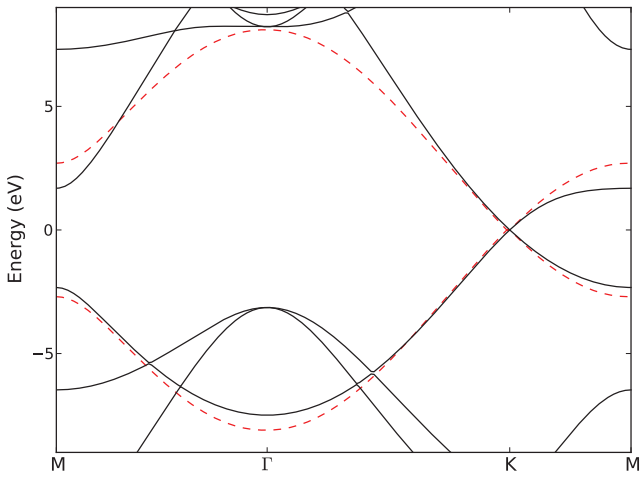

Figure 3.2. Graphene band structure between high symmetry points along the path shown in figure 3.1. Tight-binding results (dashed red) compared with DFT (solid black). The extra DFT bands are due to the σ-bonds which are ignored in the TB model.

Figure 3.2 shows a comparison between DFT (SIESTA with LDA functional) and tight-binding band structure (equation (3.2) with $t = -2.7eV$). Close to the Fermi energy the correspondence is exact, while further away there are some discrepancies. The comparison with DFT shows that a tight-binding level description should be accurate for graphene. One can however simplify even more by noticing that the dispersion is actually *linear* near the Fermi level. Linearizing (3.2) near the K-points of the reciprocal lattice gives a linear dispersion

$$E(\mathbf{k}) = \pm v_F |k| \tag{3.3}$$

with the Fermi velocity $v_F = \frac{\sqrt{3}at}{2}$.

The linear dispersion relation at the K and K' Dirac points hints at the possibility for simplifying the tight-binding model even further. One proceeds by Fourier transforming the equation (3.1) and expanding for the Dirac point only [34] to get the expression

$$-iv_F\sigma \cdot \nabla\psi(\mathbf{r}) = E\psi(\mathbf{r}), \tag{3.4}$$

for the K Dirac point. Here $\sigma = (\sigma_x, \sigma_y)$ is formed from the Pauli matrices. A similar expression can be derived for the other Dirac point. The link with relativistic field theory comes from the fact that equation (3.4) is the same as massless Dirac equation in two dimensions.

We do not employ the Dirac model for the calculations in this thesis but rather either use DFT or directly numerically solve the TB equation (3.1) and its generalizations. The use of the Dirac equation is covered in many reviews on the electronic structure of graphene [34] and electron transport in bulk graphene [35]. Some fundamental properties of charge transport are however directly related to the peculiar structure of the Hamiltonian and thus merit comment. Most importantly the eigenfunctions of (3.4) are two-component spinors, where the "spin" is not the physical spin of the electrons but rather comes from the two sublattices and is called the pseudospin. The spinor structure of the eigenfunctions has important consequences for the transport properties of the Dirac fermions. In terms of the Berry's phase it means that when the k is rotated around the origin by an angle of 2π the phase of the wavefunction changes by $-\pi$. This leads to an absence of backscattering in graphene, as pointed out first in the context of carbon nanotubes [36].

It is interesting to consider the possible deficiencies of the tight binding model for graphene. In particular electron-electron interactions can change the picture drastically by renormalizing the bands [37]. Also at very high temperatures or bias voltages phonon scattering effects become appreciable.

3.2 Graphene nanoribbons

As graphene has no band gap, several schemes to produce a gap have been proposed. These include creating a superlattice of graphene antidots or holes in graphene [38], using gated bilayer graphene [39] and the cutting of graphene into a finite-width wire, a graphene nanorib-

bon [40]. The most developed of these methods is arguably the production of graphene nanoribbons (GNR), strips of graphene with edges. In addition to lithographic patterning [40] graphene nanoribbons have also been created through chemical self-assembly [41] and the unzipping of nanotubes [42].

Ideal nanoribbons belong to one of two classes: zigzag (ZGNR) or armchair (AGNR). Figure 3.3 shows the two ribbon categories and the typical way of counting the ribbon width: by carbon dimer for AGNRs and zigzag line for ZGNRs. Somewhat confusingly if an armchair nanoribbon is made periodic in the transverse direction it will form a zigzag carbon nanotube while a zigzag nanoribbon will transform to an armchair nanotube. DFT calculations indicate that armchair edges are energetically the most stable ones [43].

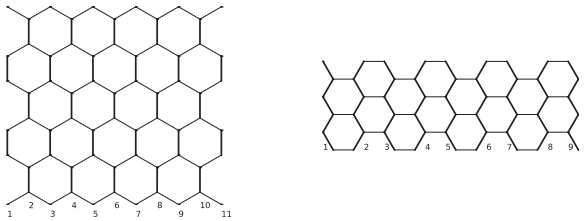

Figure 3.3. Two ideal graphene nanoribbon types: armchair (AGNR) and zigzag (ZGNR) and how the width of the ribbons are typically indexed.

If a graphene sheet is cut in some other direction than ideal armchair or zigzag, a chiral edge is the end result. Apart from the chiral and ideal edges also reconstructions of the edge shape are possible. The so called reczag reconstruction of the zigzag edge is even lower in energy than the armchair edge [44]. This edge type, which is formed by pentagons and heptagons at the graphene edge, has also been seen experimentally [45], though it appears not to be the dominant edge type. In fact, in many experiments there is a large amount of zigzag edge, even though it is much higher in energy than the armchair edge [46]. One explanation for this conundrum can be found in the kinetics of the edge carbon atoms when the edge is formed [47, 48].

The dangling bonds at the nanoribbon edge are extremely reactive and will thus almost certainly be saturated by atoms or molecules. The dangling bonds are thus commonly assumed to be saturated by hydrogen when doing theoretical calculations. It is far from clear that the edges are ideally passivated with one hydrogen atom for each dangling bond

under experimental conditions. Indeed, under many experimentally relevant conditions DFT calculations indicate that the edge is passivated by hydrogen *molecules* either at every dangling bond or at every other [49]. Also the possibility of various other edge terminations has been studied [50, 51].

Now that we have discussed some of the many difficulties inherent in the study of graphene nanoribbons, mostly related to their edges, we turn back to the most simple case of armchair and zigzag nanoribbons passivated with hydrogen. The TB model used to understand the properties of bulk graphene can be very useful for the study of ribbons as well. However for ribbons the correspondence between ab initio results and TB results turns out to be greatly inferior to the case of bulk graphene. Whereas for bulk graphene the low energy band dispersion is more or less perfectly captured by TB, DFT shows armchair ribbons of all widths to have bandgaps, while the TB model shows some widths to be metallic. For zigzag ribbons the situation is even worse since the ground state DFT result turns out to be magnetic and thus not within the validity of a standard TB treatment. The work of modifying a TB model so that it can accommodate these more complicated results for nanoribbons is the main focus of Publication II.

Figure 3.4 shows the band structures for ribbons of a particular width, a 14-AGNR and a 16-ZGNR. There is a significant difference between the TB and the DFT results shown. TB predicts that both the ZGNR and AGNR are metallic while DFT shows both to be semiconducting.

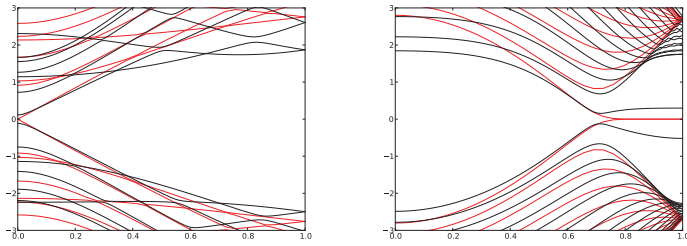

Figure 3.4. Band structure close to the Fermi energy for a 14-AGNR and 16-ZGNR calculated with the unmodified nearest neighbor tight binding model (red) and compared with a DFT calculation (black).

The natural way to improve the TB model is to increase the number of hopping elements between neighboring atoms. Whereas before we only had the nearest neighbor Hamiltonian element, we now increase up to third nearest neighbor hopping. The second way to gain greater accuracy

is to go from orthogonal to nonorthogonal tight-binding. This means that the Scrödinger equation contains the overlap matrix S

$$H\left|\psi\right\rangle = \omega_\alpha S\left|\psi\right\rangle, \tag{3.5}$$

where the matrix elements of S are

$$S_{ij} = \langle i|j\rangle, \tag{3.6}$$

over the single particle states i and j.

Zigzag nanoribbons present extra difficulties for theory due to the magnetic ordering in the ground state. DFT indicates that spin ordering with ferromagnetism along the ribbon edges and antiferromagnetism between the edges is energetically favored. This is followed by a ferromagnetic ordering between the edges and finally by the paramagnetic state [52]. The experimental evidence for the magnetic edge state remains slim, though some evidence has been seen by scanning tunneling microscopy recently [53].

To study magnetism within a TB approach one needs to leave behind the plain TB model and consider a Hubbard-type Hamiltonian that explicitly includes the spin-up and spin-down densities $n_\downarrow$ and $n_\uparrow$. The mean-field Hubbard-model Hamiltonian then reads

$$H = -\sum_{ij\sigma} t_{ij} c^\dagger_{i\sigma} c_{j\sigma} + U \sum_i \left(n_{i\uparrow}\langle n_{i\downarrow}\rangle + n_{i\downarrow}\langle n_{i\uparrow}\rangle - \langle n_{i\uparrow}\rangle\langle n_{i\downarrow}\rangle\right). \tag{3.7}$$

Here the "Hubbard" U is the onsite Coulomb repulsion between electrons of opposite spin. The brackets denote average spin density per orbital, which can be calculated from the retarded Green's function G^R by

$$\langle n_{i\sigma}\rangle = -\frac{1}{\pi}\int_{-\infty}^{E_F} \mathrm{Im}\{G^R_{\sigma ii}\}. \tag{3.8}$$

Comparing the band structure between DFT and TB and adjusting the TB parameters is done in Publication II to yield a minimal third-nearest neighbor orthogonal TB parametrization with t_1 = 2.7 eV, t_2 = 0.2 eV, t_3 = 0.18 eV and U = 2.0 eV for zigzag ribbon. This parametrization is found to generate results close to DFT results for both armchair and zigzag ribbons and it thus forms an universal minimal TB parametrization for accurate calculations of all types of ribbon systems. In addition to pristine ribbons, also ribbons with edge disorder, such as notches, are found to be described well as found out by comparing with DFT transport calculations in Publication I and Publication II.

The tight-binding parametrization presented here works quite well and yields good results. However some more complicated systems such as divacancies, due to be discussed later, are complicated to deal with on such an ad hoc basis since there are many bond lengths that change. A good alternative here is to get a bond-length dependent parametrization based on DFT calculations and then use relaxed results as input for the bond lengths. Such an approach can also be used to produce a gap for all AGNR families, as shown by Son *et al.* [54], by decreasing the hopping between edge-most carbon atoms according to DFT relaxed bond lengths.

Like the case of planar graphene also for graphene nanoribbons the possibility that electron-electron interactions might be important should be considered. We have already seen that for the case of zigzag terminations Coulomb repulsion leads to a spin-polarized ground state. We should then keep in mind that the DFT approach, using the "normal" functionals LDA and GGA at least, does not apply very well for strongly correlated electron systems. Indeed, it has been shown that adding to DFT a self-consistent GW formalism the gaps of graphene nanoribbons are significantly increased [55]. For transport the possibility of Coulomb blockade between weakly coupled graphene islands has been proposed as an explanation to transport experiments [56].

4. Defective graphene

4.1 Single defects

Although pristine graphene and ideal nanoribbons are of themselves interesting, realistic experimental systems tend to contain various defects. These generally degrade the transmission properties of graphene and understanding the main sources of defects is thus important for improving the behavior of graphene samples for graphene electronics. Although exfoliated graphene samples are remarkably defect-free based on their excellent electronic properties, defects still pose limits for ultimate graphene device performance.

One of the most widely studied defect types that has an impact on graphene transport are defects not in the graphene itself but in the insulating substrate, typically made of silicon oxide [35]. These are thought to be caused by charge trapped in the oxide and the theory is corroborated by the fact that when the oxide is removed to form *suspended* graphene the mobility is greatly increased [57]. From the point of view of theory the most salient feature of the scattering potential caused by the charges is that it is long range in nature, changing smoothly on the scale of the graphene lattice constant. Such a potential does not scatter electrons between the valleys at K and K' Dirac points, i.e., it does not cause intervalley scattering, just intravalley scattering.

One factor that affects the scattering of electrons in graphene by smooth potentials is the phenomenon of Klein tunneling. The name comes from a feature of relativistic field theory but for graphene it simply means that the charge carriers tunnel through potential barriers with a probability of one [58]. This is relevant especially for electron transport close to the Fermi energy where it has been experimentally shown that the graphene

charge density forms puddles of positive and negative charge [59] and the transport thus happens between these regions via Klein tunneling.

In addition to charges in the substrate a great deal of work has been done to understand the properties of short-range scatterers which do cause intervalley scattering. These short-range scattering centers are formed for example by vacancies and adatoms.

For better understanding of short-range scatterers such as vacancies a very useful technique is the intentional creation of defects by irradiating graphene with either electrons or ions [60]. In this manner the number and type of defects can be estimated based on known quantities such a carbon knock-off energies and irradiation doses and the transport measurements studied as a function of generated defect density. Defect creation could also be used to improve upon nanoribbon performance for some specific tasks, for example by tailoring defect centers for interaction with certain molecular species for sensor applications.

In addition to the presence of the same scattering mechanisms that exist for bulk graphene, nanoribbons have one very important additional scattering mechanism, edge disorder. The various ways of creating nanoribbons typically cannot produce exact edges but ones that are to a large extend disordered. Edge disorder has often been modeled by randomly removing edge atoms from a graphene nanoribbon with some probability p and then cleaning up probably unphysical edge shapes such as dangling atoms.

Edge disorder is particularly interesting in the case of zizgag ribbons. Breaking the symmetry between the ribbon sides can produce a spin-filtering effect. Lieb's theorem may give rise to a finite magnetic moment if the sublattice symmetry between the edges is broken [61]. Apart from simple atom-level disorder at the edge, also larger edge structures such as notches and protrusions have been studied. In Publication I we have looked into how notches affect the transmission through a zigzag ribbon. A notch in a zigzag ribbon will have an effect on just one of the spin-polarized edge states.

Point defects in the graphene bulk can take the form of adatoms of various species, vacancies (single and divacancies) and topological defects such as the Stone-Wales defect. The most widely studied of these is the single vacancy formed by removing one carbon atom. Although this is commonly modeled by simply removing the relevant hopping elements from a TB model, the reality is not so simple. Figure 4.1 shows a compar-

ison for the transmission through a nanoribbon with a vacancy calculated with (spin compensated) DFT and with TB. As can be seen from the figure the transmission through a single vacancy calculated with the TB model is much closer to the DFT calculation for a hydrogen atom adsorbed on the graphene basal plane than the DFT vacancy transmission. The reason for this discrepancy is due to the dangling bonds left after a carbon atom is removed.

Single vacancies have been studied extensively as a paradigmatic source of short-range scattering in graphene. Short-range scatterers act qualitatively differently from longer range defects such as Coulombic charges in the SiO substrate since they couple the two different valleys of graphene around the K and K' Dirac points. Their presence can be used to explain the sublinear behaviour seen in transport measurements [62]. The simple vacancy-type TB model has also been used to understand more complex cases such as graphene with substitutional Co atoms [63].

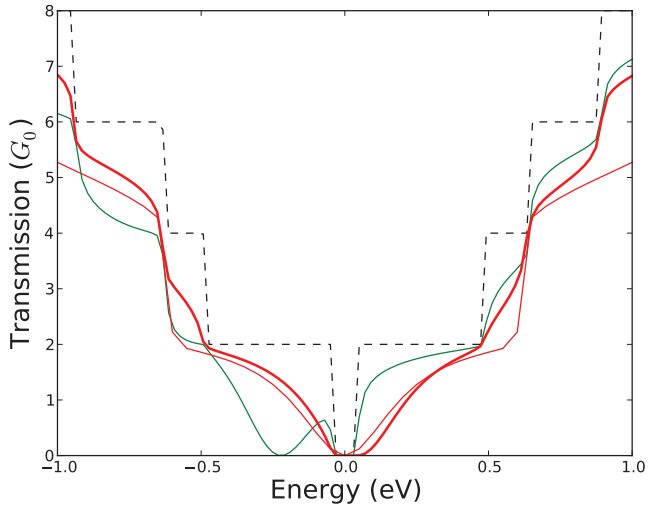

Figure 4.1. Transmission through a 23-AGNR with a vacancy modeled with DFT (thick red) and TB (green) compared with transmission though a GNR with a hydrogen atom modeled with DFT (thin red). Thin black dashed line shows the ideal transmission through the ribbon.

One important aspect for the transmission through defective nanoribbons is the sometimes fairly large impact that the precise location of the impurity on the transmission. Figure 4.2 shows the transmission through a 23-AGNR with a hydrogen atom in three different locations and the ideal transmission through a pristine ribbon. Particularly striking is the complete vanishing of the transmission dip when the defect is located on

the third carbon carbon dimer. This turns out to be a general feature for odd-width armchair nanoribbons where impurities on $3N$ indexable dimers do not scatter electrons. The reason for this can be found in the symmetries of the ribbon electron structure [64, 65].

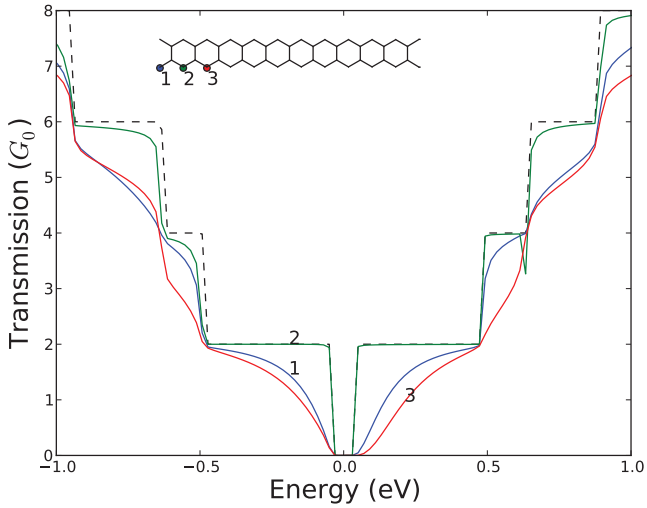

Figure 4.2. The effect of defect location on the electron transmission for a 23-AGNR with hydrogen adsorbed on different locations. The inset shows the adsorption sites across the ribbon.

One interesting aspect for single vacancies is that they are fairly mobile. In addition, since the formation of divacancies is energetically favored, one can expect clustering of vacancies into divacancies, especially under many nonequilibrium circumstances such as under ion or electron bombardment. Divacancies can undergo relaxation forming different defect structures known as 585 and 555777 divacancies, as shown in Figure 4.3. The 555777 divacancy is created from the 585 divacancy through a bond rotation. Energetically the 555777 divacancy is the most stable one [66]. The figure also shows an example of the even more complicated defect structures that can be formed though the agglomeration of divacancies, a 555567777 double divacancy.

Defects can also be formed without the removal of atoms. Most prominent of these is the topological Stone-Wales defect (SW) formed by rotating one carbon-carbon bond [67]. For all these defects, the SW, the 585, the 555777 and so on the construction of a tight-binding model is best accomplished by a parametrization based on bond length. This typically relies on DFT in two ways: first the relaxed bond lengths are taken from

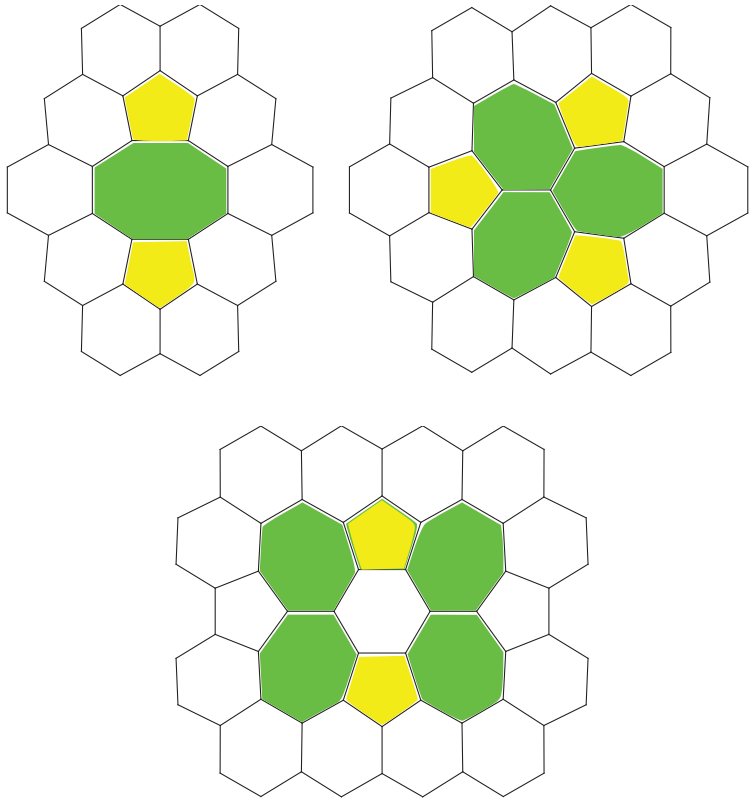

Figure 4.3. Different divacancy relaxations, the 585-divacancy, the 555777 divacancy and the 555567777 double divacancy. Pentagons are colored yellow while heptagons are colored with green.

a DFT calculation and then the distance dependent hopping elements are parametrized based on DFT calculations [68]. This procedure produces results very much comparable with DFT for the electron transmission as is discussed Publication IV.

Of the different adatom species hydrogen is most likely the most studied. At full coverage hydrogen turns graphene into graphane, a band insulator [69]. As shown before in Figure 4.1 a simple tight-binding model where a site is completely removed by removing all the hoppings to it fairly accurately corresponds with the DFT results.

The model can also be improved easily by adding a new interacting level for the hydrogen, i.e. by

$$H = \sum_{<i,j>} \left(t c_i^\dagger c_j + t c_j^\dagger c_i \right) + \varepsilon d^\dagger d + \gamma d^\dagger c_0 + \gamma c_0^\dagger d, \tag{4.1}$$

where the carbon atom with the index 0 is coupled to the impurity level. The modification introduces two parameters, the impurity energy level ε and the hybridization γ. This simple and versatile model has been widely

used to model hydrogen and various other adsorbates, such as the hydroxyl group and hydrocarbons, that bind on top of a carbon atom [70, 71, 72]. For hydrogen the parameters giving results corresponding well to DFT calculations [71] are $\gamma = 2t$ and $\varepsilon = t/16$ though other values have also been proposed [70].

Other adatoms, such as oxygen and carbon, preferentially bind on the bridge site between carbon atoms. Their modeling is thus more difficult, though they can be modeled as resonant levels, similarly to the hydrogen case discussed above.

Particularly complicated behavior can occur when looking at the effect of adsorbates and edge disorder together. In Publication III we have looked at these effects for a model system with simple protruded graphene edges and oxygen as the chemical disorder. Structural edge disorder has a fairly low impact on the armchair edge while the adsorption of oxygen generates strong antiresonances in the transmission.

Here we have concentrated on the properties of point defects in graphene. Extended defects such as dislocations have also been widely studied and present interesting properties such as strongly suppressed transmission at certain incident angles [73].

4.2 Many defects: disorder

Although two-probe calculations for single defects are instructive by themselves, typically realistic nanosystems contain more defects than just one. Let us then consider a long two-probe system with many randomly distributed defects. It is not directly clear if the single defect transmission results discussed in the previous section can be used to understand such a system.

Since the transport is coherent, interference will play a role and the transmission function depends on the precise location of each and every defect. It is not realistic to know the detailed atomistic structure of an experimental sample so the numerical results need to be averaged by performing numerous calculations for random defect locations which are then summed over.

The transmission through a long sample can be calculated recursively in linear time since a long wire can be broken into slices [74]. This makes it possible to calculate transmission through ribbons of arbitrary length even with DFT as long as they are narrow enough. The whole proce-

dure is, however, quite time consuming, especially since the transmissions should be finally averaged over the ensemble of randomly located defects. For this typically some hundreds of calculations for each studied length will need to be performed.

Figure 4.4 shows the average transmission function calculated with TB through a 41-AGNR when the single vacancy density is kept constant at 0.1 % and the distance is increased. The transmission goes steadily down and a gap appears at the Fermi level. This gap is often called a *transport* gap as opposed to the band gap or optical gap.

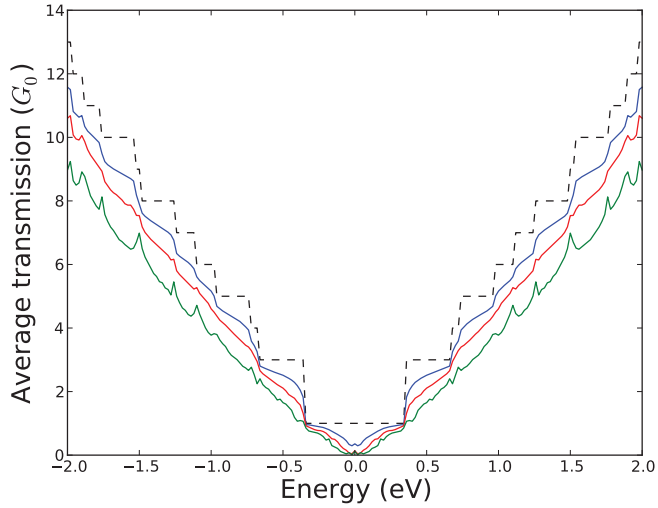

Figure 4.4. Average transmission through a 41-AGNR with single vacancies at a probability of 0.1 % at various distances. The dashed black line indicates pristine ribbon, blue line is for L=10 nm, red line for L=20 nm and green line for L=40 nm.

Ideally we would like to go from the single-defect transmission calculations discussed in the last section to a large-system-averaged limit. It turns out that this can be accomplished with scaling theory.

The study of disordered electron systems forms a large and interesting field of its own due to some interesting theoretical findings. Philip W. Anderson showed in 1958 [75] that the eigenfunctions of a random lattice decay exponentially in a strong enough disorder leading to a metal-insulator transition. This is nowadays understood as general feature of coherent transmission through a disordered medium that has been experimentally observed in thin metal films for electrons and photonic crystals for coherent light [76].

Even before Anderson localization takes place, disorder can have an in-

terference effect on transmission. This is called weak localization as it precedes the strong or Anderson localization. It can be intuitively understood by the fact that for systems with time-reversal symmetry there is a constructive interference between the time reversed transmission paths. This leads to a lowering of the transmission from the incoherent transmission, a fact that can be experimentally probed by introducing a magnetic field to break the time-reversal symmetry.

Scaling theory deals with the change in transmission when the size of the sample is increased. It has been studied in different dimensions analytically and there are many reviews of the techniques and findings [77, 78, 79, 80]. We have studied the scaling properties of long disordered graphene nanoribbons in Publication IV and generalized the previous work done on silicon nanowires [81, 82].

We will illustrate the concept of scaling numerically with the TB model by looking at the resistance through a long nanoribbon as a function of ribbon length in Figure 4.5. The ribbon has a density of vacancy defects with probability 1 % per carbon atom. First there are no defects and the transmission is just the transmission through the ideal system $T = T_0$. The corresponding resistance is called the contact resistance $R = R_c = 1/T_0$ since its physical origin is the mismatch between the continuum of conducting states in the leads and the finite number of transverse states inside the ballistic conductor.

As the length of the ribbon increases the resistance starts to increase linearly

$$R(L) = R_c + R_c \frac{L}{l_e}, \tag{4.2}$$

where the characteristic length l_e defines the elastic mean free path and it characterizes the strength of the elastic scatterers in the system. The resistance is calculated by averaging, $R = 1/\langle T \rangle$, where the brackets denote ensemble averaging. This is a well-defined operation for the transmission as it has a Gaussian distribution around the average value as is shown in the inset in figure 4.5. This regime is known as diffusive or Ohmic regime since the resistance grows linearly as for macroscopic Ohmic conductors.

We can solve for the elastic mean free path

$$l_e = \frac{R_c}{\langle R \rangle - R_c} L = \frac{\langle T \rangle}{\langle T \rangle - T_0} L. \tag{4.3}$$

The greater the amount of defects the smaller the elastic mean free path. So to characterize the scattering strength of a defective region of size $W \times L$ with a defect density of $n = N/WL$ we define the Ohmic scattering

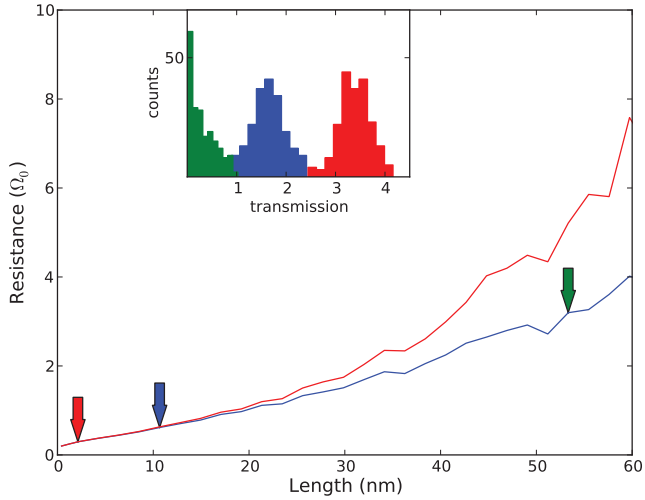

Figure 4.5. Resistance of a 41-AGNR at a particular energy (E=0.8 eV) as a function of ribbon length. The resistance is calculated by $R = 1/\langle T \rangle$ for the blue curve and $R = 1/\exp\langle \ln(T) \rangle$ for the red curve. The resistance shows three distinct regimes: ballistic regime where the resistance remains constant, diffusive regime where the resistance grows linearly and finally localized regime where the resistance increases exponentially. The inset shows the statistical distribution of the transmission at the lengths indicated by the arrows, showing the evolution from the Gaussian to the log-normal distribution.

cross-section

$$\sigma(\omega) = \frac{1}{nl_e(\omega)} = W\frac{T_0(\omega) - \langle T(\omega)\rangle}{N\langle T(\omega)\rangle}. \tag{4.4}$$

For our purposes the most interesting usage of this equation is calculating the scattering cross-section from an ensemble of single-defect transmission calculations like those discussed previously. Then $N = 1$ and we average over all the distinct defect locations and orientations across the ribbon.

We can use the scattering cross-section to find the elastic mean free path or the averaged transmission

$$\langle T(\omega)\rangle = \frac{T_0(\omega)}{1 + L\sum_i n_i\sigma_i(\omega)}, \qquad L \ll \xi(\omega). \tag{4.5}$$

This means that it is feasible to go from the single defect transmission results directly to the limit of large samples.

When the length of the ribbon increases the resistance starts to increase superlinearly. This shows the onset of Anderson localization. The transmission is no longer Gaussian but log-normal [83]. This is shown in the inset histogram of figure 4.5 and by the fact that resistance calculated from the average transmission (blue curve) and the exponent of the aver-

age logarithm of the transmission start to diverge.

This means that the averaging should be done over the logarithm of the transmission by $\langle \ln T(\omega) \rangle$ and one should look at the scaling of the typical transmission $T_{typ} = \exp(\langle \ln T(\omega) \rangle)$. For a conductor with one mode it can be shown [83] that $T_{typ}(\omega) \propto \exp(-L/\xi(\omega))$ so for a lead with multiple modes we arrive at the expression

$$T_{typ}(\omega) = T_0(\omega) \exp(-L/\xi(\omega)). \tag{4.6}$$

This regime of transport is called localized, strongly localized or Anderson localized and the length ξ the localization length. Since it is also determined by the strength of the elastic scattering it is possible to find it from the elastic mean free path. This can be done by using random matrix theory [79, 84] and turns out to depend on the symmetry of the Hamiltonian. For graphene with intervalley scattering, which belongs to the orthogonal Wigner-Dyson symmetry class when there is no external magnetic field, we get the expression

$$\xi(\omega) = \frac{(T_0(\omega)+1) l_{el}(\omega)}{2} = \frac{T_0(\omega)+1}{2n\sigma(\omega)}, \tag{4.7}$$

which leads us to a definition of the scattering cross-section for the localized regime

$$\sigma(\omega) = \frac{W(T_0(\omega)+1)\langle \log(T_0(\omega)/T(\omega)) \rangle}{2N}, L \gg \xi(\omega). \tag{4.8}$$

For using single defect calculations we generally do not need to use this equation, though in some rare cases even one defect is enough to localize the charge carriers of the lowest transmission mode. More usefully we can find out the typical transmission from the scattering cross-section

$$T_{\mathrm{typ}}(\omega) = \frac{T_0(\omega)}{\exp\left[\frac{2L}{T_0(\omega)+1} \sum_i n_i \sigma_i(\omega)\right]}, \quad L \gg \xi(\omega). \tag{4.9}$$

Equation 4.9 along with (4.5) allows us to estimate the average or typical transmission from the scattering cross section for ribbons of arbitrary length. The scattering cross-section then fully determines the average behavior of charge carriers for a defective sample.

The discussion above has been about the localization behaviour in ribbons with short range disorder. In bulk graphene with long-range disorder the localization behavior is quite different. As discussed before, long-range disorder does not couple the two valleys and so a two component spinor description is possible. Then the Berry's phase of π between time-reversed trajectories will cause *destructive* instead of constructive interference leading to weak antilocalization for the Dirac electrons. As there

might be also short-range scattering present this leads to a complex interplay between localization and antilocalization behavior depending on the amount of different types of disorder and the experimental situation is currently far from clear [35].

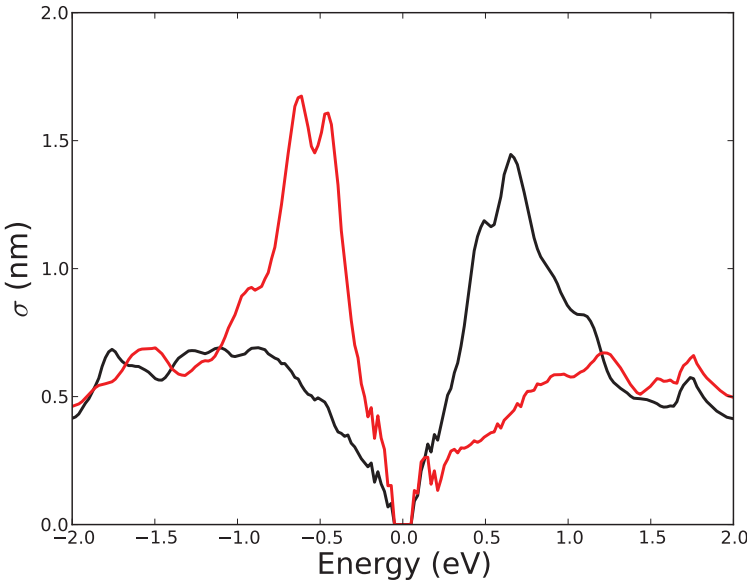

Figure 4.6. Scattering cross-section for carbon (red) and oxygen (black) adatoms in bulk graphene calculated for a periodic graphene sheet corresponding to a 32-AGNR.

The scattering cross-section of the previous equations is based on calculating the transmission for a finite width ribbon. It can also be calculated for a periodic system, however, thus forming a quantity that characterizes the defect itself with no connection to a ribbon of particular width. We studied the cross-sections in Publication V for various adatoms in bulk and ribbon geometries. Figure 4.6 illustrates the idea of the scattering fingerprint by showing the scattering cross-sections for oxygen and carbon adatoms calculated for a bulk graphene systems corresponding to a 32-AGNR. The scattering cross-section for both of these bridge adsorbed species is highly characteristic: for oxygen it is peaked above the Fermi energy while for carbon a similar peak exists below the Fermi energy. Similar characteristic defect fingerprints have been calculated for single and divacancies in Publication IV.

Figure 4.7 shows the estimation of transmission through a defective sample with the aid of the scattering cross section using the Ohmic (equation (4.5)) and localized (equation (4.9)) formulas. It shows that the transmission through a large sample containing many different defect species

can be very accurately predicted just based on single-defect scattering cross sections and that this works for systems of any size, both within the Ohmic and localized regimes.

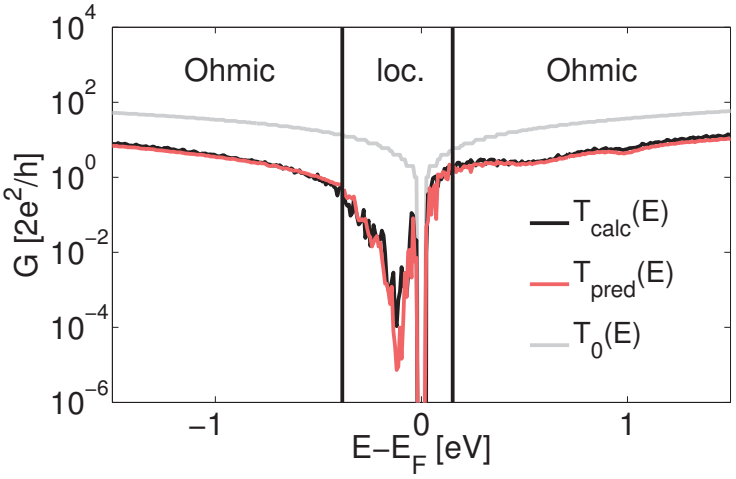

Figure 4.7. Averaged transmission (T_{calc}) through a 1.3 μm long and 30 nm wide AGNR with 100 monovacancies, Stone-Wales defects and 555777 defects. Comparison with a prediction for the Ohmic and localized regimes based on a scattering cross-section.

5. Summary and Conclusions

This thesis presented a computational study of graphene based on DFT calculations and a DFT-parametrized TB model. The main focus was on defective nanoribbons and their study with a combination of first-principles and TB numerical calculations. DFT is fairly slow but accurate method for electronic structure calculations whereas TB is the opposite. They thus form an ideal pair for the study of complicated and realistic graphene samples.

Although plain nearest-neighbor TB is quite accurate for the case of bulk graphene, it turns out to be unsatisfactory for graphene nanoribbons. For nanoribbons it can however be easily expanded by taking second and third nearest neighbors into account and optionally also considering finite overlap elements between the orbitals. For magnetic systems one can utilize the Hubbard model where different spins have a local Coulombic repulsion and the density distribution of the spins is then found self consistently. The extended TB model was shown to be nearly as accurate as DFT for the case of pristine and edge-defective ribbons.

For more complicated disordered systems, DFT is very useful since it is typically not clear how exactly one should parameterize the TB or the Hubbard model. This is especially the case for adatoms. In the presence of both adatoms and edge disorder very complicated phenomena can be seen.

DFT is not typically very suitable for studying long disordered graphene samples due to the high use of computational resources. Although these can be modeled with the aid of TB a DFT level treatment is very useful for adatoms and other cases where the parametrization is not evident. As the study of long disordered samples is done by averaging over an ensemble of different defect positions we can use a scaling approach to go from single-defect results to macroscopic samples. We have shown that this

approach is usable for both different types of vacancy defects, topological Stone-Wales defects and adatoms. The scaling approach also works in the localized regime, thus making it possible to use DFT single-defect transmission results directly for ribbons of arbitrary length with a high degree of accuracy. Although the defect transmission fingerprint should be in principle be calculated for each ribbon width separately, in practice good results are gained for wide ribbons by calculating the transmission through a periodic graphene sample for which the scattering cross-section thus forms a defect fingerprint.

Bibliography

[1] Novoselov, K. S., Geim, A. K., Morozov, S. V., *et al.* Electric Field Effect in Atomically Thin Carbon Films. Science, **306**:666 (2004).

[2] Geim, A. Nobel Lecture: Random walk to graphene. Reviews of Modern Physics, **83**:851 (2011).

[3] Novoselov, K. Nobel Lecture: Graphene: Materials in the Flatland. Reviews of Modern Physics, **83**:837 (2011).

[4] Novoselov, K. S., Geim, A. K., Morozov, S. V., *et al.* Two-dimensional gas of massless Dirac fermions in graphene. Nature, **438**:197 (2005).

[5] Zhang, Y., Tan, Y.-W., Stormer, H. L., and Kim, P. Experimental observation of the quantum Hall effect and Berry's phase in graphene. Nature, **438**:201 (2005).

[6] Wallace, P. R. The Band Theory of Graphite. Phys. Rev., **71**:622 (1947).

[7] Semenoff, G. W. Condensed-Matter Simulation of a Three-Dimensional Anomaly. Physical Review Letters, **53**:2449 (1984).

[8] López Sancho, M., López Sancho, J., and Rubio, J. Quick iterative scheme for the calculation of transfer matrices: application to Mo (100). Journal of Physics F: Metal Physics, **14**:1205 (1984).

[9] Sorensen, H. H. B., Hansen, P. C., Petersen, D. E., Skelboe, S., and Stokbro, K. Krylov subspace method for evaluating the self-energy matrices in electron transport calculations. Physical Review B, **77**:155301 (2008).

[10] Datta, S. *Electronic Transport in Mesoscopic systems*, volume 3 of *Cambridge Studies in Semiconductor Physics and Microelectronic Engineering*. Cambridge University Press (1997).

[11] Caroli, C., Combescot, R., Nozieres, P., and Saint-James, D. Direct calculation of the tunneling current. Journal of Physics C: Solid State Physics, **4**:916 (1971).

[12] Fisher, D. S. and Lee, P. A. Relation between conductivity and transmission matrix. Physical Review B, **23**:6851 (1981).

[13] Fiolhais, C., Nogueira, F., and Marques, M. A., editors. *A Primer in Density Functional Theory*. Springer-Verlag (2003).

[14] Kresse, G. and Hafner, J. Ab initio molecular dynamics for liquid metals. Physical Review B, **47**:558 (1993).

[15] Mortensen, J. J., Hansen, L. B., and Jacobsen, K. W. Real-space grid implementation of the projector augmented wave method. Physical Review B, **71**:35109 (2005).

[16] Moreno, J. and Soler, J. M. Optimal meshes for integrals in real- and reciprocal-space unit cells. Physical Review, **45**:13891 (1992).

[17] Ordejón, P., Artacho, E., and Soler, J. M. Self-consistent order-N density-functional calculations for very large systems. Physical Review B, **53**:R10441 (1996).

[18] Soler, J. M., Artacho, E., Gale, J. D., *et al.* The SIESTA method for ab initio order-N materials simulation. Journal of Physics: Condensed Matter, **14**:2745 (2002).

[19] Monkhorst, H. and Pack, J. Special points for Brillouin-zone integrations. Physical Review B, **13**:5188 (1976).

[20] Brandbyge, M., Mozos, J.-L., Ordejón, P., Taylor, J., and Stokbro, K. Density-functional method for nonequilibrium electron transport. Physical Review B, **65**:165401 (2002).

[21] Rungger, I. and Sanvito, S. Algorithm for the construction of self-energies for electronic transport calculations based on singularity elimination and singular value decomposition. Physical Review B, **78**:35407 (2008).

[22] Mostofi, A. A., Yates, J. R., Lee, Y.-S., *et al.* wannier90: A tool for obtaining maximally-localised Wannier functions. Computer Physics Communications, **178**:685 (2008).

[23] Ishii, H., Triozon, F., Kobayashi, N., Hirose, K., and Roche, S. Charge transport in carbon nanotubes based materials: a KuboâĂŞGreenwood computational approach. Comptes Rendus Physique, **10**:283 (2009).

[24] Lherbier, A., Biel, B., Niquet, Y.-M., and Roche, S. Transport Length Scales in Disordered Graphene-Based Materials: Strong Localization Regimes and Dimensionality Effects. Physical Review Letters, **100**:36803 (2008).

[25] Moser, J., Tao, H., Roche, S., *et al.* Magnetotransport in disordered graphene exposed to ozone: From weak to strong localization. Physical Review B, **81**:205445 (2010).

[26] Leconte, N., Lherbier, A., Varchon, F., *et al.* Quantum transport in chemically modified two-dimensional graphene: From minimal conductivity to Anderson localization. Physical Review B, **84**:235420 (2011).

[27] Evers, F. and Burke, K. Pride, Prejudice, and Penury of ab initio transport calculations for single molecules (2006).

[28] Koentopp, M., Chang, C., Burke, K., and Car, R. Density functional calculations of nanoscale conductance. Journal of Physics: Condensed Matter, **20**:083203 (21pp) (2008).

[29] di Ventra, M. *Electrical Transport in Nanoscale Systems*. Cambridge University Press (2008).

[30] Stefanucci, G. and Almbladh, C.-O. Time-dependent partition-free approach in resonant tunneling systems. Physical Review B, **69**:195318 (2004).

[31] Cini, M. Time-dependent approach to electron transport through junctions: General theory and simple applications. Physical Review B, **22**:5887 (1980).

[32] Kurth, S., Stefanucci, G., Almbladh, C.-O., Rubio, A., and Gross, E. K. U. Time-dependent quantum transport: A practical scheme using density functional theory. Physical Review B, **72**:35308 (2005).

[33] Thygesen, K. S. and Rubio, A. Conserving GW scheme for nonequilibrium quantum transport in molecular contacts. Physical Review B, **77**:115333 (2008).

[34] Castro Neto, A. H., Guinea, F., Peres, N. M. R., Novoselov, K. S., and Geim, A. K. The electronic properties of graphene. Reviews of Modern Physics, **81**:109 (2009).

[35] Das Sarma, S., Adam, S., Hwang, E., and Rossi, E. Electronic transport in two-dimensional graphene. Reviews of Modern Physics, **83**:407 (2011).

[36] Ando, T., Nakanishi, T., and Saito, R. Berry's Phase and Absence of Back Scattering in Carbon Nanotubes. Journal of the Physical Society of Japan, **67**:2857 (1998).

[37] Kotov, V., Uchoa, B., Pereira, V., Guinea, F., and Castro Neto, A. Electron-Electron Interactions in Graphene: Current Status and Perspectives. Reviews of Modern Physics, **84**:1067 (2012).

[38] Pedersen, T. G., Flindt, C., Pedersen, J., *et al.* Graphene Antidot Lattices: Designed Defects and Spin Qubits. Physical Review Letters, **100**:136804 (2008).

[39] Castro, E. V., Novoselov, K. S., Morozov, S. V., *et al.* Biased Bilayer Graphene: Semiconductor with a Gap Tunable by the Electric Field Effect. Physical Review Letters, **99**:216802 (2007).

[40] Han, M. Y., Ozyilmaz, B., Zhang, Y., and Kim, P. Energy Band-Gap Engineering of Graphene Nanoribbons. Physical Review Letters, **98**:206805 (2007).

[41] Li, X., Wang, X., Zhang, L., Lee, S., and Dai, H. Chemically Derived, Ultrasmooth Graphene Nanoribbon Semiconductors. Science, **319**:1229 (2008).

[42] Jiao, L., Zhang, L., Wang, X., Diankov, G., and Dai, H. Narrow graphene nanoribbons from carbon nanotubes. Nature, **458**:877 (2009).

[43] Okada, S. Energetics of nanoscale graphene ribbons: Edge geometries and electronic structures. Physical Review B, **77**:41408 (2008).

[44] Koskinen, P., Malola, S., and Häkkinen, H. Self-Passivating Edge Reconstructions of Graphene. Physical Review Letters, **101**:115502 (2008).

[45] Koskinen, P., Malola, S., and Häkkinen, H. Evidence for graphene edges beyond zigzag and armchair. Physical Review B, **80**:73401 (2009).

[46] Girit, C. O., Meyer, J. C., Erni, R., *et al.* Graphene at the Edge: Stability and Dynamics. Science, **323**:1705 (2009).

[47] Jia, X., Hofmann, M., Meunier, V., *et al.* Controlled Formation of Sharp Zigzag and Armchair Edges in Graphitic Nanoribbons. Science, **323**:1701 (2009).

[48] Engelund, M., Fürst, J. A., Jauho, A.-P., and Brandbyge, M. Localized Edge Vibrations and Edge Reconstruction by Joule Heating in Graphene Nanostructures. Physical Review Letters, **104**:36807 (2010).

[49] Wassmann, T., Seitsonen, A. P., Saitta, A. M., Lazzeri, M., and Mauri, F. Structure, Stability, Edge States, and Aromaticity of Graphene Ribbons. Physical Review Letters, **101**:96402 (2008).

[50] Cervantes-Sodi, F., Csányi, G., Piscanec, S., and Ferrari, A. C. Edge-functionalized and substitutionally doped graphene nanoribbons: Electronic and spin properties. Physical Review B, **77**:165427 (2008).

[51] Seitsonen, A., Saitta, A., Wassmann, T., Lazzeri, M., and Mauri, F. Structure and stability of graphene nanoribbons in oxygen, carbon dioxide, water, and ammonia. Physical Review B, **82**:115425 (2010).

[52] Pisani, L., Chan, J. A., Montanari, B., and Harrison, N. M. Electronic structure and magnetic properties of graphitic ribbons. Physical Review B, **75**:64418 (2007).

[53] Tao, C., Jiao, L., Yazyev, O. V., *et al.* Spatially resolving edge states of chiral graphene nanoribbons. Nature Physics, **7**:616 (2011).

[54] Son, Y.-W., Cohen, M. L., and Louie, S. G. Energy gaps in graphene nanoribbons. Physical Review Letters, **97**:216803 (2006).

[55] Yang, L., Park, C.-H., Son, Y.-W., Cohen, M. L., and Louie, S. G. Quasiparticle Energies and Band Gaps in Graphene Nanoribbons. Physical Review Letters, **99**:186801 (2007).

[56] Sols, F., Guinea, F., and Castro Neto, A. H. Coulomb Blockade in Graphene Nanoribbons. Physical Review Letters, **99**:166803 (2007).

[57] Bolotin, K. I., Sikes, K. J., Jiang, Z., *et al.* Ultrahigh electron mobility in suspended graphene. Solid State Commun., **146**:351 (2008).

[58] Katsnelson, M. I., Novoselov, K. S., and Geim, A. K. Chiral tunnelling and the Klein paradox in graphene. Nature Physics, **2**:620 (2006).

[59] Martin, J., Akerman, N., Ulbricht, G., *et al.* Observation of electron-hole puddles in graphene using a scanning single-electron transistor. Nature Physics, **4**:144 (2008).

[60] Banhart, F., Kotakoski, J., and Krasheninnikov, A. V. Structural defects in graphene. ACS Nano, **5**:26 (2011).

[61] Lieb, E. H. Two theorems on the Hubbard model. Physical Review Letters, **62**:1201 (1989).

[62] Ferreira, A., Viana-Gomes, J., Nilsson, J., *et al.* Unified description of the dc conductivity of monolayer and bilayer graphene at finite densities based on resonant scatterers. Physical Review B, **83**:165402 (2011).

[63] Santos, E. J. G., Sánchez-Portal, D., and Ayuela, A. Magnetism of substitutional Co impurities in graphene: Realization of single π vacancies. Physical Review B, **81**:125433 (2010).

[64] Deretzis, I., Fiori, G., Iannaccone, G., and La Magna, A. Effects due to backscattering and pseudogap features in graphene nanoribbons with single vacancies. Physical Review B, **81**:85427 (2010).

[65] Choe, D. H., Bang, J., and Chang, K. J. Electronic structure and transport properties of hydrogenated graphene and graphene nanoribbons. New Journal of Physics, **12**:125005 (2010).

[66] Kotakoski, J., Krasheninnikov, A., Kaiser, U., and Meyer, J. From Point Defects in Graphene to Two-Dimensional Amorphous Carbon. Physical Review Letters, **106**:1 (2011).

[67] Kotakoski, J., Meyer, J., Kurasch, S., *et al.* Stone-Wales-type transformations in carbon nanostructures driven by electron irradiation. Physical Review B, **83**:1 (2011).

[68] Porezag, D., Pederson, M. R., and Liu, A. Y. Importance of nonlinear core corrections for density-functional based pseudopotential calculations. Physical Review B, **60**:14132 (1999).

[69] Elias, D. C., Nair, R. R., Mohiuddin, T. M. G., *et al.* Control of Graphene's Properties by Reversible Hydrogenation: Evidence for Graphane. Science, **323**:610 (2009).

[70] Robinson, J. P., Schomerus, H., Oroszlány, L., and Fal'ko, V. I. Adsorbate-Limited Conductivity of Graphene. Physical Review Letters, **101**:196803 (2008).

[71] Wehling, T., Yuan, S., Lichtenstein, A., Geim, A., and Katsnelson, M. Resonant Scattering by Realistic Impurities in Graphene. Physical Review Letters, **105**:056802 (2010).

[72] Yuan, S., De Raedt, H., and Katsnelson, M. Modeling electronic structure and transport properties of graphene with resonant scattering centers. Physical Review B, **82**:115448 (2010).

[73] Yazyev, O. V. and Louie, S. G. Electronic transport in polycrystalline graphene. Nature materials, **9**:806 (2010).

[74] Markussen, T., Rurali, R., Brandbyge, M., and Jauho, A.-P. Electronic transport through Si nanowires: Role of bulk and surface disorder. Physical Review B, **74**:245313 (2006).

[75] Anderson, P. Absence of Diffusion in Certain Random Lattices. Physical Review, **109**:1492 (1958).

[76] Akkermans, E. and Montambaux, G. *Mesoscopic Physics of Electrons and Photons*. Cambridge University Press (2007).

[77] Lee, P. A. and Ramakrishnan, T. V. Disordered electronic systems. Reviews of Modern Physics, **57**:287 (1985).

[78] Kramer, B. and MacKinnon, A. Localization:theory and experiment. Reports on Progress in Physics, **56**:1469 (1993).

[79] Beenakker, C. Random-matrix theory of quantum transport. Reviews of Modern Physics, **69**:731 (1997).

[80] Evers, F. and Mirlin, A. Anderson transitions. Reviews of Modern Physics, **80**:1355 (2008).

[81] Markussen, T., Rurali, R., Jauho, A.-P., and Brandbyge, M. Scaling theory put into practice: First-principles modeling of transport in doped silicon nanowires. Physical Review Letters, **99**:76803 (2007).

[82] Markussen, T., Rurali, R., Cartoixà, X., Jauho, A.-P., and Brandbyge, M. Scattering cross section of metal catalyst atoms in silicon nanowires. Physical Review B, **81**:125307 (2010).

[83] Anderson, P., Thouless, D., Abrahams, E., and Fisher, D. New method for a scaling theory of localization. Physical Review B, **22**:3519 (1980).

[84] Beenakker, C. W. J. Applications of random matrix theory to condensed matter and optical physics (2009).

Aalto-DD 7/2013

ISBN 978-952-60-4965-6
ISBN 978-952-60-4966-3 (pdf)
ISSN-L 1799-4934
ISSN 1799-4934
ISSN 1799-4942 (pdf)

Aalto University
School of Science
Department of Applied Physics
www.aalto.fi

BUSINESS + ECONOMY

ART + DESIGN + ARCHITECTURE

SCIENCE + TECHNOLOGY

CROSSOVER

DOCTORAL DISSERTATIONS